RSC Advances

ROYAL SOCIETY OF CHEMISTRY

www.rsc.org/advances

Cite this: DOI: 10.1039/c0xx00000x

www.rsc.org/xxxxxx

Communication

Mesoporous VO_2 Nanowires with Excellent Cycling Stability and Enhanced Rate Capability for Lithium Battery

Lei Zhang,‡ Kangning Zhao,‡ Wangwang Xu, Jiashen Meng, Liang He* Qinyou An, Xu Xu, Yanzhu Luo, Tingwei Zhao and Liqiang Mai*

Received (in XXX, XXX) Xth XXXXXXXXX 20XX, Accepted Xth XXXXXXXXX 20XX
DOI: 10.1039/b000000x

To combine merits of the one-dimensional structure and the porous structure, mesoporous VO_2 nanowires have been designed and reported for the first time. Excellent cycling stability and enhanced rate performance is obtained and may be attributed to the mesoporous nanowire, realizing both high surface area for more active sites and facile stress relaxation resulting in excellent structure stability. Our results demonstrate that the mesoporous nanowire is favourable for high-rate and long-life lithium batteries.

Introduction

Nowadays, the ever-increasing energy demand for new, sustainable and environment-friendly energy sources has been a vital and challenging issue [1-6]. Among those various available energy storage technologies, rechargeable lithium batteries (LBs) have received great interests due to their high energy density, long lifespan and no memory effect [7-14]. However, LBs fall short of the ever-increasing energy demands from large scale applications, such as electrical vehicles and grid-level energy storage. In order to meet the requirements of large scale applications, high power density is urgently required [15-20]. Thus, it is of great significance to search for ideal electrode materials realizing high energy density and power density. Vanadium oxides are among the best cathode materials for rechargeable lithium batteries, due to both their large specific capacity and abundant sources. VO_2 (B) is one of most attractive electrode materials owing to the advantageous feature of double layers of V_4O_{10} type for fast lithium intercalation/deintercalation[21-24]. However, the low diffusion coefficient of lithium ions (10^{-9} – 10^{-10} cm^2 s^{-1}) [25-26] and limited cycling stability [27-31] hinder the practical applications of this material.

Designing electrode materials within nanoscale has been regarded as one of the most efficient method in fabricating ideal electrodes [32-34]. Compared with bulk materials, nanowires are able to exhibit the advantages of both facile strain relaxation upon charging/discharging related to long cycle life and large surface to volume ratio to increase the contact area between the electrolyte and electrode. Nanowires as building blocks with complex structures and multiple functionalities have been reported to demonstrate the superior electrochemical performance in energy storage applications [35-40]. In our previous work, constructing pores through top-down method in microplates has been demonstrated to be an efficient approach in fabricating electrode with excellent rate capability and stable capacity [41]. Thus, constructing pores in nanowire will be a more efficient method because it can not only utilize superiorities of one-dimensional structure, but also take the advantages of mesoporous structure, such as good access of the electrolyte to the electrode surface, large surface area facilitating charge transfer across the electrode/electrolyte interface, increased utilization of active material and suppressed phase transformations and structure degradations during cycling [42-45]. However, as is well known, nanowires due to the high reactivity are challenging to create pores without damaging the mechanical integrity. Thus, controllable and rational pores construction in nanowire has been a challenging issue.

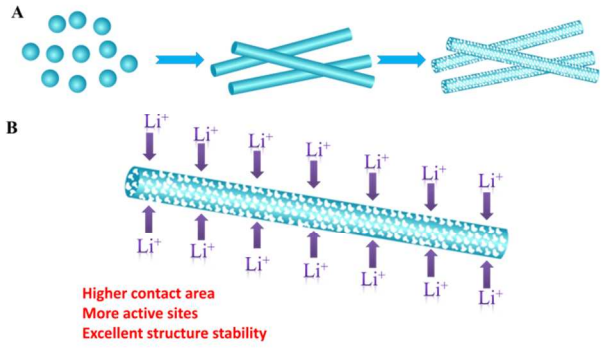

Figure 1. Schematic illustrations of the fabrication steps and proposed formation mechanism of the mesoporous nanowires (A) and mesoporous nanowires offer high contact area, more active sites and excellent structural stability during lithium insertion/deinsertion (B).

Herein, to combine both merits of nanowire and mesoporous structure, a facile method preparing mesoporous VO_2 nanowires is reported via hydrothermal process and solid state reaction. $NH_4V_3O_8$ nanowires is obtained through the condensation of the vanadium precursor[45] via hydrothermal method. Through annealing method, the $NH_4V_3O_8$ nanowires is decomposed leading to internal gas emitting from inside and surface of the nanowire. The pressure of the internal gas may create interconnected pore networks, leading to the unique open pore distribution. In this way, the mesoporous VO_2 nanowires are

achieved. Benefiting from the 1D structure and the tunable interconnected porosity, such unique architecture may greatly enhance the electrochemical performance in terms of specific capacity, cycling stability and rate capability.

Experimental Section

Materials synthesis

In a typical synthesis, NH_4VO_3 (9 mmol) was dissolved in deionized water (40 mL) at 80 °C. The pH of the solution was adjusted to 2 by adding 5% hydrogen chloride solution. After stirring for two hours, the solution was then transferred to autoclave at 180 °C for 7 days. The precipitation was washed with water and alcohol for several times to get the $NH_4V_3O_8$ nanowires. Subsequently, the mesoporous VO_2 nanowires were obtained by annealing the as-prepared $NH_4V_3O_8$ nanowires in N_2 atmosphere at 400 °C for 4 h at the heating rate of 10 °C/min. The non-mesoporous VO_2 nanowires were obtained through oxalic acid reduction method. In a typical synthesis, the V_2O_5 powder (2 mmol) and oxalic acid (3.6 mmol) were dissolved in 33 mL water. The solution was then transferred into autoclave at 180 °C for 24 hours. The precipitation was then washed with water and alcohol for several times and dryed at 60 °C for 8 h to obtain the non-mesoporous VO_2 nanowires.

Characterization

X-ray diffraction (XRD) measurements were performed to investigate the crystallographic information using a D8 Advance X-ray diffract meter with non-monochromatic Cu Kα X-ray 15 source. Field emission scanning electron microscopic (FESEM) images were collected with a JEOL JEM-7100F microscopy at an acceleration voltage of 10 kV. Transmission electron microscopic (TEM) images and high-resolution transmission electron microscopic (HRTEM) images were recorded by using a JEOL JEM-2100F FEF microscope. Brunauer–Emmet–Teller (BET) surface areas were measured using Tristar II 3020 instrument to investigate the adsorption of nitrogen. X-ray photoelectron spectroscopy (XPS) is carried out by using KRATOS XSAM800 electron spectrometer.

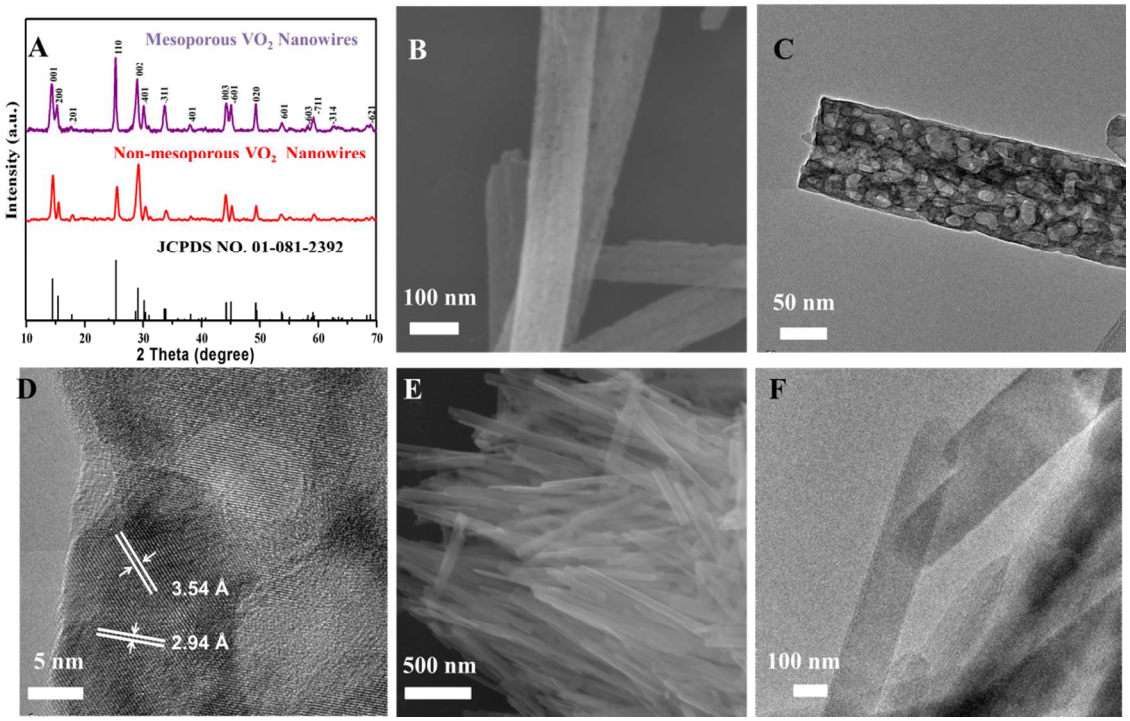

Figure 2. (A) XRD patterns of non-mesoporous VO_2 nanowires (red), mesoporous VO_2 nanowire (purple); SEM image (B), TEM image (C) and HRTEM image (D) of mesoporous VO_2 nanowire; SEM images (E) and TEM image (F) of non-mesoporous VO_2 nanowires.

Measurement of Electrochemical Performance

The electrochemical properties were carried out by assembly of 2025 and 2016 coin cells in a glove box filled with pure argon gas. Lithium pellet was used as the anode; 1 M solution of $LiPF_6$ in ethylene carbon (EC)/dimethyl carbonate (DMC) as electrolyte. Cathode electrodes were obtained with 70% mesoporous VO_2 nanowires as active material, 20% acetylene black and 10% poly (tetrafluoroethylene) (PTFE). Galvanostatic charge/discharge cycling was studied in a potential range of 2.0 - 3.0 V *vs*. Li/Li^+ with a multichannel battery testing system (LAND CT2001A). Cyclic voltammetry (CV) and AC-impedance spectra were tested with an electrochemical workstation (CHI 760D and Autolab PGSTAT 302).

Results and Discussion

The schematic illustration of formation process is shown in Figure 1. During the first process, the condensation of the vanadium precursor goes via oxalation as well as preferably via the faster olation reaction along the H_2O–V–OH direction and leads to the formation of 1D vanadium oxide within the xy plane

[46]. During the second step, through different annealing temperature, the different valence of vanadium is obtained (Fig. S8). The $NH_4V_3O_8$ nanowires were decomposed into mesoporous VO_2 nanowires under annealing process at annealing temperature of 450 ^oC via the reaction (1):

$$NH_4V_3O_8 \rightarrow 3VO_2 + 2H_2O + \frac{1}{2}N_2 \quad (1)$$

Owing to the gas emitting, the pores are interconnected and the nanowire is composed of many small pores. The vanadium oxide which blocks the gas from generating is induced by H_2O and N_2, leading to the pores both on the surface and the inner side of the nanowires. The interconnected porosity can lead to high surface area and, in this way, is able to offer more active sites and shorten the lithium diffusion distance for lithium insertion/deinsertion (Figure 1B). Moreover, the porous structure may create void for facile stress relaxation in lithium insertion/deinsertion.

The products were characterized by XRD (Figure 2A) to identify the crystallographic structure and crystallinity. It can be observed that the precursor can be identified to monoclinic $NH_4V_3O_8$ (JCPDS NO. 01-089-6614, space group: P21/m, a = 4.9993 Å, b = 8.4230 Å, c = 7.8490 Å) (Figure S1), and the patterns of the mesoporous VO_2 nanowires and the non-mesoporous VO_2 nanowires can both be indexed as monoclinic VO_2 (JCPDS NO. 01-081-2392, space group: C2/m, a = 12.0930 Å, b = 3.7021 Å, c = 6.4330 Å). Moreover, the XPS spectrum confirmed that the valence of the vanadium is +4 (Fig. S9). Monoclinic $NH_4V_3O_8$ consists of the interconnection of the VO_5 square pyramids and VO_6 octahedra within one V_3O_8 layer. The layers are stacked along the c-direction with the NH^{4+} cations occupying the interlayer space which may be suitable for the generation of N_2 and H_2O while retaining the morphology[47-49]. Monoclinic VO_2 consists of double layers of V_4O_{10} type [26]. According to the *o-t-o* diffusion [50], the NH^{4+} ion occupies a cubic close packed lattice of octahedral sites offering higher energy barrier. Thus, better electrochemical performance of mesoporous VO_2 nanowires is expected than that of $NH_4V_3O_8$ nanowires (Figure S2).

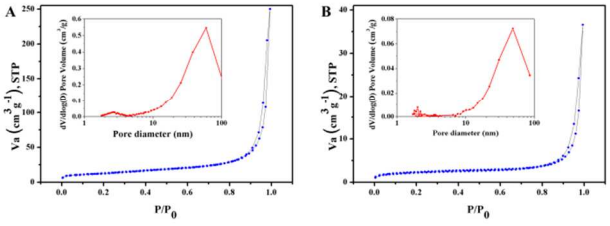

Figure 3. Nitrogen adsorption and desorption isotherms and pore size distribution (Inset) of mesoporous (A) and non-mesoporous (B) VO_2 nanowires.

SEM and TEM techniques were further applied to characterize the morphology and detailed structure of the as-prepared samples. As shown in the SEM image, the precursor $NH_4V_3O_8$ nanowires are randomly placed and the diameter of the nanowires is in the range of 80-100 nm (Figure S3). After annealing, the mesoporous VO_2 nanowires retain the morphology with 120 nm in diameter, indicating that upon the emitting of internally born nitrogen and water, the diameter of the nanowire expands in the annealing process (Figure 2B). Pores about 20 nm can be easily observed both inside and on the surface of the VO_2 nanowires (Figure 2C). In order to further identify the pore size and the structure of the mesoporous VO_2 nanowires, HRTEM is carried out (Figure 2D). The good crystallinity of mesoporous VO_2 nanowires was confirmed by HRTEM. The lattice fringe spacings of 2.94 and 3.53 Å are recognized, corresponding to the (111) and (110) plane of VO_2, respectively, as confirmed by the XRD pattern (Figure 2A). As shown in Figure 2E, the non-mesoporous VO_2 nanowires are also 120 nm in diameter. On the surface of the non-mesoporous nanowires, no obvious pore is observed (Figure 2F). Thus, without undergoing the decomposition process, the non-mesoporous VO_2 nanowires show no signs that pores are on the surface or inside the solid nanowires.

BET is an efficient tool to identify the pore distribution. The N_2 adsorption desorption isotherms and the corresponding Barrett–Joyner–Halenda (BJH) pore-size distributions of mesoporous VO_2 nanowires are shown in Figure 3. The mesoporous VO_2 nanowires illustrate typical type-IV N_2 absorption isotherms with distinct H3 hysteresis loops that can be linked to slit-shaped pores, contributing very high surface area of 46.7 m^2/g (Figure 3A), which is over two times as large as the precursor $NH_4V_3O_8$ nanowires (15.1 m^2/g) (Figure S4), more than five times as high as non-mesoporous VO_2 nanowires (8.0 m^2/g) (Figure 3B). The pore size distribution is among 30 nm in diameter. When compared to the $NH_4V_3O_8$ nanowires and the non-mesoporous VO_2 nanowires, the mesoporous VO_2 nanowires exhibits much higher pore volume (0.6 cm^3/g), which is five times and ten times higher than that of $NH_4V_3O_8$ nanowires (0.12 cm^3/g) and non-mesoporous VO_2 nanowires (0.06 cm^3/g), respectively, indicating that the highest pore volume may be attributed to the pores in mesoporous VO_2 nanowires. The resulting large surface area may provide more active sites for lithium intercalation and deintercalation, which may result in better electrochemical performance.

Coin cells of metallic lithium as anode were assembled to investigate the electrochemical performance of as-prepared samples. As shown in the CV curves, a pair of redox peaks occurs (Figure 4A) when cycled between 2 and 3 V, corresponding to the reaction (2)[26]:

$$VO_2 + x\mathrm{Li}^+ + xe^- = \mathrm{Li}_xVO_2 \quad (2)$$

The difference in anodic and cathodic peaks is due to the polarization of the as-prepared samples. In order to evaluate the polarization, the overpotential is calculated from the difference between charge potential and discharge potential at the half reversible capacity, noted as $\Delta V(Q/2)$.[26] The overpotential of mesoporous nanowires (0.23 V) is much lower than that of non-mesoporous nanowires (0.36 V), indicating excellent reversibility. The CV curves match well with the charge-discharge voltage profiles (Figure 4B). And during the first three cycles, the shapes of the charge-discharge curves are almost identical, indicating excellent reversibility of the lithium insertion/deinsertion process. The result shows that the discharge-charge curves are almost superposed during first three cycles. One voltage plateau is clearly observed which is quite consistent with the CV curves. The cycling performance at different current densities ranging from 100 mA/g to 1000 mA/g is performed. At the current density of 100 mA/g, the mesoporous VO_2 nanowires deliver initial discharge capacity of 188 mAh/g which is a bit higher than that of non-mesoporous nanowires (175 mAh/g) (Figure 4C). The

capacity of mesoporous VO_2 nanowires witnesses no obvious decay after 100 cycles with discharge capacity of 180 mAh/g, corresponding to capacity retention of 95%, exhibiting excellent cycling stability, much higher than that of non-mesoporous VO_2 nanowires (78%). At current density of 500 mA/g, the initial capacities of both samples show greater difference (Figure 4D). The initial discharge capacity of mesoporous VO_2 nanowires (143 mAh/g) is much higher than that of non-mesoporous nanowires (116 mAh/g). After 300 cycles, the capacity of mesoporous VO_2 nanowires is 127 mAh/g, corresponding to 89% of its initial capacity. On the contrast, non-mesoporous VO_2 nanowires fade fast to below 100 mAh/g after 100 cycles. All these indicate that the mesoporous VO_2 nanowires show excellent cycling stability.

Further, at high current density of 1000 mA/g, each sample, during first cycle, delivers a discharge capacity of 105 and 84 mAh/g, respectively, demonstrating even greater difference in initial capacity between mesoporous and non-mesoporous VO_2 nanowires (Figure 4E). Mesoporous VO_2 nanowires demonstrate excellent stability with a discharge capacity of 95 mAh/g, corresponding to 90% of its initial capacity after 500 cycles which is far higher than that of non-mesoporous nanowires (75%). Obviously, the mesoporous VO_2 nanowires exhibit higher capacity and better cycling performance than non-mesoporous VO_2 nanowires at both low and high current density.

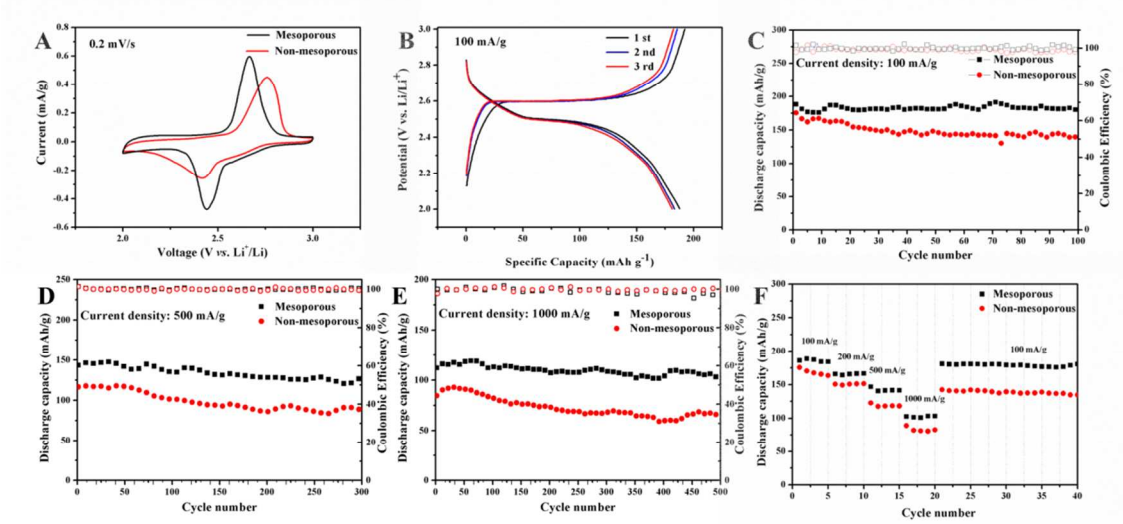

Figure 4 (A) CV curves of mesoporous and non-mesoporous VO_2 nanowires at scan rate of 0.2 mV/s; (B) charge and discharge curves of mesoporous VO_2 nanowires during the first three cycles at 100 mA/g; Cycling performance of mesoporous and non-mesoporous VO_2 nanowires at different current densities of 100 mA/g (C), 500 mA/g (D), and 1000 mA/g (E); (F) rate performance of mesoporous and non-mesoporous VO_2 nanowires.

The rate capability is a significant evaluation in lithium battery. Thus, both mesoporous and non-mesoporous VO_2 nanowires were cycled at various current density ranging from 100, 200, 500 1000 mA/g and finally back to 100 mA/g. The mesoporous VO_2 nanowires is with a discharge capacity of 186, 165, 141, 101 and 180 mAh/g (Figure 4F), which exhibits higher capacity than that of non-mesoporous VO_2 nanowires (175, 150, 122, 82 and 142 mAh/g). The capacity retention is higher than those of mesoporous nanowires. All these indicate that even after suffering from rapid change of the current density, the electrode exhibits more stable and higher capacity at each current, indicating a degree of mechanical integrity during Li ion inseriton/deinsertion process. When the current returns to 100 mA/g, about 96% of the initial capacity is recovered and there is no obvious capacity loss during the following 20 cycles. Our results demonstrate the excellent rate capability and structural stability of mesoporous VO_2 nanowires. EIS is a powerful tool to reveal the kinetics of the lithium ion extraction/insertion process which is related to the electron transport and lithium ion diffusion length[51]. EIS of mesoporous and non-mesoporous VO_2 nanowires is carried out. In this circuit, R_s represents the Ohmic resistance of the electrode system, including the electrolyte and the cell components. R_{ct} represents the charge transfer resistance. CPE and Z_w are the double layer capacitance and the Warburg impedance [51], respectively. All the Nyquist plots are composed of a depressed semicircle in the medium-frequency region followed by a slanted line in the low-frequency region (Figure S5). The mesoporous VO_2 nanowires show a much lower resistance of 40 Ω when compared with non-mesoporous VO_2 nanowires (68 Ω), indicating that the mesopores indeed enhances the charge transfer and modifies the kinetics of VO_2 mesoporous nanowires.

To explain the electrochemical results, it is important to consider the one-dimensional mesoporous structure that exerts such a significant influence on enhanced electrochemical performance. Three possible factors may result in the enhanced cycle stability and rate capability. First, the performance is related to the high surface area. The high surface area of mesoporous nanowires (46.71 m^2/g), which is 5 times higher than non-mesoporous nanowires, is attributed to the pores in the surface and inside of the nanowires. The hierarchal interconnected pores are able to offer more active sites on the surface or near-surface region for lithium intercalation/deintercalation[1]. Second, according to the diffusion formula $t = L^2/D$ (where t is the diffusion time, L is the diffusion length and D is the diffusion constant) [25], the shorter diffusion length will provide less diffusion time, leading to better electrochemical property. The mesopores in the nanowire shorten the Li^+ diffusion distance, strongly increase the lithium mobility and modify the kinetics of the lithium intercalation/deintercalation. Third, this kind of hierarchical structure shows that the mesoporous nanowires

restrain the aggregation of nanowires and offer facile stress relaxation to accommodate the volume variations. Thus, this kind of unique pore structure provides more active sites and keeps the surface area larger to make full use of the advantages of nanostructured materials.

Conclusions

Mesoporous VO_2 nanowires have been designed and prepared through facile hydrothermal method followed by annealing process. The thermal decomposition of $NH_4V_3O_8$ to generate nitrogen and water vapor creates to disordered interconnected mesopores. Thus, high specific surface area (46.7 m^2/g) is achieved. When evaluated as cathode for lithium batteries, mesoporous VO_2 nanowires exhibits stable cycling performance and excellent rate capability, thus is regarded as a promising candidate for lithium batteries. The capacity of mesoporous VO_2 nanowires witness no obvious decay after 100 cycles with discharge capacity of 180 mAh/g, corresponding to capacity retention of 95%, exhibiting much higher capacity and better capacity retention than those of non-mesoporous VO_2 nanowires (174 mAh/g and 78%), respectively. Mesoporous VO_2 nanowires exhibit a discharge capacity of 104.7 mAh/g at the current density of 1000 mA/g, and 90% of its initial capacity is retained after 500 cycles which is almost two times as high as the capacity of non-mesoporous VO_2 nanowires. This superior performance may benefit from the mesopores, which shorten ion transport route and modify the kinetics during intercalation/deintercalation. Moreover, the disordered interconnected pores are able to offer more active sites for lithium intercalation/deintercalation. Therefore, the facile and effective method can be extended to fabricate nanopores in nanomaterials and constructing this kind of unique one-dimensional mesoporous structure can be utilized for further operation in the fields of energy storage and transportation, such as Li-air battery.

Acknowledgements

This work was supported by the National Basic Research Program of China (2013CB934103, 2012CB933003), the International Science & Technology Cooperation Program of China (2013DFA50840), National Natural Science Foundation of China (51072153, 51272197) and the Fundamental Research Funds for the Central Universities (2014-IV-062, 2014-VII-007, 2014-YB-001, 2014-YB-002, 2014-ZY-016). Thanks to Prof. C. M. Lieber of Harvard University and Prof. Dongyuan Zhao of Fudan University for strong support and stimulating discussion.

Notes and references

[a] *WUT-Harvard Joint Nano Key Laboratory, State Key Laboratory of Advanced Technology for Materials Synthesis and Processing, , Wuhan University of Technology, Wuhan, 430070, P. R. China. Fax: +86-027-87644867; Tel: +86-027-87467595; E-mail:* mlq518@whut.edu.cn and hel@whut.edu.cn

† Electronic Supplementary Information (ESI) available.
See DOI: 10.1039/b000000x/

‡ Author contributions: Lei Zhang, Kangning Zhao contributed equally to this work. All authors discussed the results and commented on the manuscript.The authors declare no competing financial interest.

1. P. Simon, Y. Gogotsi and B. Dunn, *Science*, 2014, **343,** 1210.
2. F. Y. Cheng, J. Liang, Z. L. Tao and J. Chen, *Adv. Mater.*, 2011, **23**, 1695.
3. A. Yoshino, *Angew. Chem. Int. Ed*, 2012, **51**, 5798.
4. M. Armand and J. M. Tarascon, *Nature*, 2008, **451**, 652.
5. H. G. Jung, M. W. Jang, J. Hassoun, Y. K. Sun and B. Scrosati. *Nat. Commun.*, 2011, **2,** 516.
6. H. G. Zhang, X. D. Yu and P. V. Braun, *Nat. Nanotech.*, 2011, **6**, 277.
7. J. Chen and F. Y. Cheng, *Acc. Chem. Res.*, 2009, **42**, 713.
8. Y. G. Wang, H. Q. Li, L. P. He, E. J. Hosono and H. S. Zhou, *Nanoscale*, 2010, **2**, 1294.
9. H. Wu, G. Chan, J. W. Choi, I. Ryu, Y. Yao, M. T. McDowell, S. W. Lee, A. Jackson, Y. Yang, L. B. Hu and Y. Cui, *Nat. Nanotech.*, 2012, **7**, 310.
10. T. Sasaki, Y. Ukyo and P. Novak, *Nat. Mater.*, 2013, **12**, 569.
11. N. Liu, Z. D. Lu, J. Zhao, M. T. McDowell, H. W. Lee, W. Zhao and Y. Cui, *Nat. Nanotech.*, 2014, **9**, 187.
12. M. M. O. Thotiyl, S. A. Freunberger, Z. Q. Peng, Y. H. Chen, Z. Liu and P. G. Bruce, *Nat. Mater.*, 2013, **12**, 1050.
13. J. H. Kong, W. A. Yee, Y. F. Wei, L. P. Yang, J. M. Ang, S. L. Phua, S. Y. Wong, R. Zhou, Y. L. Dong, X. Li and X. H. Lu, *Nanoscale*, 2013, **5**, 2967.
14. J. Bai, X. G. Li, G. Z. Liu, Y. T. Qian and S. L. Xiong, *Adv. Funct. Mater.*, 2014, DOI: 10.1002/adfm.201303442.
15. J. B. Goodenough and K. S. Park, *J. Am. Chem. Soc.*, 2013, **135**, 1167.
16. H. S. Zhou, *Energy Environ. Sci.*, 2013, **6**, 2256.
17. Y. Y. Hu, Z. G. Liu, K. W. Nam, O. J. Borkiewicz, J. Cheng, X. Hua, M. T. Dunstan, X. Q. Yu, K. M. Wiaderek, L. S. Du, K. W. Chapman, P. J. Chupas, X. Q. Yang and C. P. Grey, *Nat. Mater.*, 2013, **12**, 1130.
18. F. Zhang, T. F. Zhang, X. Yang, L. Zhang, K. Leng, Y. Huang and Y. S. Chen, *Energy Environ. Sci.*, 2013, **6**, 1623.
19. S. De, P. W. C. Northrop, V. Ramadesigan and V. R. Subramanian, *J. Power Sources*, 2013, **227**, 161.
20. Y. L. Zhao, L. Xu, L. Q. Mai, C. H. Han, Q. Y. An, X. Xu, X. Liu and Q. J. Zhang, *Proc. Natl. Acad. Sci. USA*, 2012, **109**, 19569.
21. K. Tang, X. K. Mu, P. A. van Aken, Y. Yu, J. Maier, *Adv. Energy Mater*, 2013, **3**, 49.
22. Z. Y. Zhou, N. Tian, J. T. Li, I. Broadwell and S. G. Sun, *Chem. Soc. Rev.*, 2011, **40**, 4167.
23. J. B. Rivest and P. K. Jain, *Chem. Soc. Rev.*, 2013, **42**, 89.
24. S. Li, Y. F. Dong, D. D. Wang, W. Chen, L. Huang, C. W. Shi and L. Q. Mai, *Front. Phys*., 2013,1.
25. S. B. Yang, Y. J. Gong, Z. Liu, L. Zhan, D. P. Hashim, L. L. Ma, R. Vajtai and M. Ajayan, *Nano Lett.*, 2013, **13**, 1596.
26. L. Q. Mai, Q. L. Wei, Q. Y. An, X. C. Tian, Y. L. Zhao, X. Xu, L. Xu, L. Chang and Q. J. Zhang, *Adv. Mater.*, 2013, **25**, 2969.
27. A. Q. Pan, H. B. Wu, L. Yu and X. W. Lou, *Angew. Chem.*, 2013, **125**, 2282.
28. C. Nethravathi, C. R. Rajamathi, M. Rajamathi, U. K. Gautam, X. Wang, D. Golberg and Y. Bando, *ACS Appl. Mater. Interfaces*, 2013, **5**, 2708.
29. H. Q. Li, P. He, Y. G. Wang, E. Hosonoa and H. S. Zhou, *J. Mater. Chem.*, 2011, **21**, 10999.
30. Y. Wang, K. Takahashi, K. H. Lee and G. Z. Cao, *Adv. Funct. Mater.*, 2006, **16**, 1113.
31. D. W. Liu, Y. Y. Liu, A. Q. Pan, K. P. Nagle, G. T. Seidler, Y. H. Jeong and G. Z. Cao, *J. Phys. Chem. C*, 2011, **115**, 4959.
32. L. Li, T. Y. Zhai, Y. Bando and D. Golberg, *Nano Energy*, 2012, **1**, 91.
33. C. Zhou , Y. W. Zhang, Y. Y. Li and J. P. Liu, *Nano Lett.*, 2013, **13**, 2078.
34. B. Liu, X. L. Hu, H. H. Xu, W. Luo, Y. M. Sun and Y. H. Huang, *Sci. Rep.*, 2014, **4**, 4229.
35. L. Li, H. Lu, Z. Y. Yang, L. M. Tong, Y. Bando, and D. Golberg, *Adv. Mater.*, 2013, **25**, 1109.
36. Y. Yao, N. Liu, M. T. McDowell, M. Pastaa and Y. Cui, *Energy Environ. Sci.*, 2012, **5**, 7927.
37. L. Q. Mai, F. Yang, Y. L. Zhao, X. Xu, L. Xu, Lin and Y. Z. Luo, *Nat. Commun.*, 2011, **2**,381.

38. N. Liu, Y. Yao, J. J. Cha, M. T. McDowell, Y. Han and Y. Cui, *Nano Research*, 2012, **5**, 109.
39. Z. Li, L. X. Yuan, Z. Q. Yi, Y. Liu, Y. Xin, Z. L. Zhang and Y. H. Huang, *Nanoscale*, 2014, **6**, 1653.
40. J. H. Son, J. Wei, D. Cobden, G. Z. Cao and Y. N. Xia, *Chem. Mater.*, 2010, **22**, 3043.
41. Q. Y. An, P. F. Zhang, Q. L. Wei, L. He, F. Y. Xiong, J. Z. Sheng, Q. Q, Wang and L. Q. Mai, *J. Mater. Chem. A.*, 2014, **2**, 3297.
42. B. Kong, J. Tang, Z. X. Wu, J. Wei, H. Wu, Y. C. Wang, G. F. Zheng and D. Y. Zhao, *Adv. Mater.*, 2014, **53**, 2888.
43. Z. S. Wu, Y. Sun, Y. Z. Tan, S. B. Yang, X. L. Feng and K. Mullen, *J. Am. Chem. Soc.*, 2012, **134**, 19532.
44. V. Augustyn, J. Come, M. A. Lowe, J. W. Kim, P. L. Tabberna, S. H. Tolbert, H. D. Abruna, P. Simon and B. Dunn, *Nat. Mater.*, 2013, **12**, 518.
45. D. W. Liu, B. B. Garcia, Q. F. Zhang, Q. Guo, Y. H. Zhang, S. Sepehri and G. Z. Cao, *Adv. Mater.*, 2009, **19**, 1015.
46. G. S. Zakharova, C. Taschner, T. Kolb, A. Leonhardt, B. Buchner and R. Klingeler, *Dalton Trans.*, 2013, **42**, 4897.
47. S. P. D. Huang and Y. K. Shan, *Chem, Commun.*, 1998, **8**, 1069.
48. B. Z. Lin and S. X. Liu, *Acta Cryst.*, 1999, **C55**, 1963.
49. L. Q. Mai, C. S. Lao, B. Hu, J. Zhou, Y. Y. Qi, W. Chen, E. D. Gu, and Z. L. Wang, *J. Phys. Chem. B* ,2006, **110**, 18138.
50. J. Lee, A. Urban, X. Li, D. Su, G. Hautier and G. Ceder, *Science*, 2014, **343**, 519.
51. X. L. Wu, Y. G. Guo, J. Su, J. W. Xiong, Y. L. Zhang and L. J. Wan, *Adv. Energy Mater.*, 2013, **3**, 1115.